Available online at www.sciencedirect.com
SCIENCE DIRECT®
Journal of Catalysis 235 (2005) 79–91
JOURNAL OF CATALYSIS
www.elsevier.com/locate/jcat

Catalytic links among the water–gas shift, water-assisted formic acid decomposition, and methanol steam reforming reactions over Pt-promoted thoria

Gary Jacobs [a], Patricia M. Patterson [a], Uschi M. Graham [a], Adam C. Crawford [a], Alan Dozier [b], Burtron H. Davis [a,*]

[a] *Center for Applied Energy Research, 2540 Research Park Drive, Lexington, KY 40511, USA*
[b] *University of Kentucky Electron Microscopy Center, Chemical and Materials Engineering Dept., A004 ASTeCC Building 0286, Lexington, KY 40506, USA*

Received 3 May 2005; revised 1 July 2005; accepted 7 July 2005

Available online 19 August 2005

Abstract

Implied in the proposed water–gas shift (WGS) mechanisms for Pt/ceria and Pt/thoria catalysts is the presumption that reduced defect centers are formed on the surface. This X-ray absorption near-edge spectroscopy study provides direct results indicating that Pt facilitates reduction in the surface shell of thoria. Mechanistic arguments from in situ diffuse reflectance infrared Fourier transform spectroscopy (DRIFTS) are provided suggesting that the active sites for WGS, water-assisted formic acid decomposition, and methanol steam reforming are associated with oxygen-deficient centers. In all cases, a high H_2O/reactant (i.e., carbon monoxide, formic acid, or methanol) ratio was used. For WGS, CO reacted with type II bridging OH groups at reduced centers to generate surface formate intermediates, the decomposition of which is suggested to be the rate-limiting step by the observation of a normal kinetic isotope effect (NKIE) associated with the formate coverage as monitored by DRIFTS under steady-state conditions using $CO + H_2O$ and $CO + D_2O$ feeds. The same NKIE was observed in steady-state reaction tests. Formic acid dissociated on the surface of thoria to yield the same surface formate species as observed when CO adsorbs. An identical NKIE associated with formate decomposition was observed when switching from a feed containing $HCOOH + H_2O$ and $DCOOH + H_2O$, establishing two important commonalities: (1) similarity in the mechanistic pathway and (2) importance of the role of type II bridging OH groups at reduced centers in the catalysis. Methanol steam reforming likely proceeded through a mechanism involving adsorption at reduced centers to generate type II methoxy species, with subsequent conversion to formate, unidentate carbonate, and finally CO_2. The higher NKIE when switching between H-labeled and D-labeled feeds suggests that conversion of methoxy species to formate may be the rate-limiting step. The methanol steam reforming reaction was selective to CO_2 at low conversion, but CO selectivity increased at higher conversions, suggesting competition with the secondary reaction of reverse WGS at higher temperature. Pt/thoria was more selective at higher conversion for CO_2 than a similarly loaded Pt/ceria catalyst. These results suggest that from a mechanistic standpoint, the two materials are virtually analogs of one another.

Keywords: Pt; Thoria; Ceria; Water–gas shift; Formic acid; Methanol; Steam reforming

1. Introduction

Pt/thoria is an active catalyst for the water–gas shift (WGS) reaction and exhibits some important similarities to Pt/ceria [1]. For example, for both materials, OH groups with band locations at lower wavenumbers associated with reduced surface centers (i.e., oxygen deficiencies or vacancies) have been reported [2–15]. That is, the bands are positioned at lower wavenumbers relative to those occurring on the fully oxidized surfaces. They are often assigned to the category of "bridging OH" or "type II." During reduction of the oxide surface shell in H_2 [1–15], or after the dissociation of H_2O

* Corresponding author.
E-mail address: davis@caer.uky.edu (B.H. Davis).

0021-9517/$ – see front matter
doi:10.1016/j.jcat.2005.07.010

after reduction with CO [14], the OH groups form two distinct bands in the infrared spectrum, recently termed types II A and II B [7]. We and others [1,11–15] have found that the addition of a noble metal, such as Rh or Pt, promotes the formation of type II OH groups at a low temperature relative to the unpromoted oxide.

Ceria has been well characterized, and it is well established that reduced centers at the surface are involved in the catalysis. Although some researchers favor a redox mechanism to explain the catalysis of WGS [16–20] and others favor a formate-based mechanism [1,11–15], at this time there is a general consensus that reduced centers are involved in the catalysis of both schemes, which are delineated as follows:

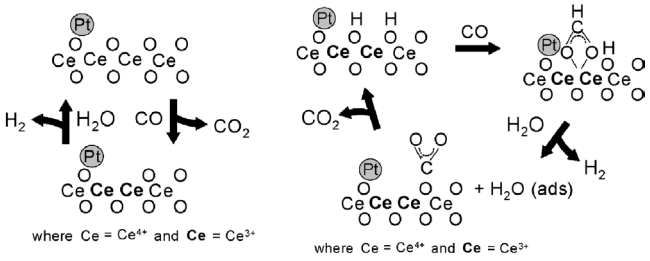

The redox mechanism proposes that the oxidation state of Ce changes between Ce^{4+} and Ce^{3+} during the course of the mechanism, with CO reducing ceria to generate CO_2 and H_2O reoxidizing ceria to liberate H_2. But there is considerable evidence suggesting that bridging OH groups on the surface react with CO to generate surface formates, which decompose in the presence of H_2O to liberate H_2 and produce unidentate carbonate, which decomposes to CO_2. Decomposition of formate in the formate mechanism promoted by H_2O; this is why H_2O was included in the transition state of the formate decomposition step of an early formate mechanism [12].

The formation of bridging OH groups can follow one of two routes on Pt/ceria:

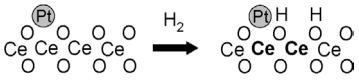

(1)

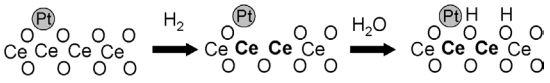

(2)

During activation, a reducing gas can remove oxygen at the surface, accompanied by a change in the oxidation state of the Ce involved from Ce^{4+} to Ce^{3+}. H_2O then dissociates on the surface to yield the bridging OH groups, but the oxidation state of the Ce involved remains Ce^{3+}. In the second case, H_2 dissociation on Pt and spillover to ceria can directly yield the bridging OH groups, again accompanied by a change in the oxidation state of the Ce involved from Ce^{4+} to Ce^{3+}.

Identification of the type II bridging OH groups on ceria was made by infrared spectroscopy; bands formed at low wavenumbers (ca. 3650 cm^{-1}) and comparatively similar bands have been observed on thoria [1–4]. We promoted thoria with Pt and found that the bridging OH group formation is facilitated by the presence of a noble metal promoter and that Pt/thoria displays high activity for WGS, comparable with Pt/ceria [1]. Intense surface formates were generated on CO adsorption to the H_2-treated catalyst, and at high H_2O/CO feed ratios, the surface concentration of formates was regulated by the WGS rate, suggesting that formates are likely intermediates for WGS over Pt/thoria as well.

Implicit in both the redox and formate mechanistic schemes is the presumption that Pt promotes the reduction of surface defects on the oxide. In the redox mechanism, the implication is that O deficiencies are created during the reduction half-reaction. In the case of the formate mechanism, formation of bridging OH groups, the active sites of that proposed mechanism, are interpreted to be dissociated H_2O at oxygen-deficient sites in the oxide surface shell. The present study presents direct results in support of oxygen deficiencies in thoria by XANES spectroscopy, provides evidence for the existence of type II bridging OH groups associated with those centers using infrared spectroscopy, explores the role of these OH groups for a number of reactions, and establishes important links among the catalytic reactions of WGS, water-assisted formic acid decomposition, and steam reforming of methanol. The study uses in situ DRIFTS spectroscopy in conjunction with reaction tests using isotope switching to probe the reaction mechanisms.

2. Experimental

2.1. Catalyst preparation

High-surface-area (BET SA = 165 m^2/g) thoria was prepared by homogeneous precipitation of thorium nitrate using urea to slowly release the precipitating agent, OH^- [1]. Details of the procedure have been reported elsewhere [1,21].

2.2. X-ray absorption near-edge spectroscopy

X-ray absorption near-edge spectroscopy (XANES) spectra at the Th L_{III} edge (16300.3 eV) were recorded at the National Synchrotron Light Source (NSLS) at Brookhaven National Laboratory, Upton, New York at beamline X-18b. A crystal detuning procedure was used to prevent glitches arising from harmonics. The second crystal of the channel-cut monochromator is weakly linked to the crystal and slightly spring-loaded. The other side is a picomotor, a very-fine high-pitch screw that turns by piezo, which allows for slight detuning of the crystal. The X-ray ring at the NSLS has a flux of 1×10^{10} photons/s at 100 mA and 2.8 GeV, and the energy range capability at X18b is 5.7–40 keV. The catalyst or standard was mixed with boron nitride (1:10) and gently pressed into a self-supporting disk and loaded into an in situ XAS cell. The samples were treated with a hydrogen/helium mixture (150 cm^3/min H_2 and 500 cm^3/min He)

while being heated at 10 °C/min in the temperature range 20–500 °C. Scans were obtained at 100 °C intervals to explore the changes in the white line intensity and binding energy during H_2 treatment. The UHP H_2 and He gases mixed in a manifold and passed through an oxygen/water trap before entering the cell. Raw data were processed to provide the normalized XANES spectra using WinXAS [22].

2.3. Temperature-programmed reduction and thermogravimetric analysis

Temperature-programmed reduction (TPR) experiments on unpromoted and 1% Pt/thoria catalysts were conducted in previous work [1]. Temperature-programmed treatment was also carried out in this study using a Seiko Instruments TG/DTA 320 simultaneous thermogravimetric/differential thermal analyzer coupled to a MICROMASS PC residual gas analyzer. A known quantity of catalyst (ca. 100 mg) was placed in a Pt sample pan and heated at 10 °C/min to 750 °C in a reducing flow of 20% v/v H_2/He after incorporating a hold at 100 °C for 30 min to dry the sample, while monitoring the effluent gas over the mass range 10–100.

2.4. Diffuse reflectance infrared Fourier transform spectroscopy

Diffuse reflectance infrared Fourier transform spectroscopy (DRIFTS) was performed with a Nicolet Nexus 870 equipped with a DTGS-TEC detector. A high-pressure/high-temperature chamber fitted with ZnSe windows was used as the WGS reactor for in situ reaction measurements. The gas lines leading to and from the reactor were heat traced, insulated with ceramic fiber tape, and further covered with general purpose insulating wrap. Scans were taken at a resolution of 4 to give a data spacing of 1.928 cm^{-1}. Typically, 128 scans were taken to improve the signal to noise ratio. The sample amount used was 33 mg.

A vaporizer was used, consisting of a downflow tube packed with quartz beads and quartz wool heated by a ceramic fiber oven equipped with an internal thermocouple. The lines after addition of liquid (e.g., water, formic acid/water mixture, or methanol/water mixture) were heat-traced to prevent condensation. Liquid was pumped into the vaporizer by a precision ISCO Model 500D syringe pump through a thin needle welded to a 1.6-mm line.

Feed gases (UHP) were controlled using Brooks 5850 series E mass flow controllers. Iron carbonyl traps consisting of lead oxide on alumina (Calsicat) were placed on the CO gas line. All gas lines were filtered with Supelco O_2/moisture traps.

2.5. Testing in a fixed-bed reactor

Steady-state conversion, selectivity, and product yield measurements were conducted with a fixed-bed reactor consisting of a 0.5-inch stainless steel tube with an internal thermocouple. The sample amount was 33 mg of catalyst diluted with 0.4 g of silica. The catalyst was supported on a bed of quartz glass wool. The vaporizer, gas delivery system, and ancillary equipment were as described in Section 2.4.

2.6. Selection of appropriate conditions

2.6.1. Steady-state measurements

2.6.1.1. Catalytic activity tests in the fixed-bed reactor Measurements were conducted at comparable reactant feed molar compositions to build mechanistic relationships among the different reactions investigated. High H_2O/reactant feed ratios were used, because we are establishing low-temperature WGS as the basis for comparison among the different reactions. In all tests, 3.75 cm^3/min of carbon monoxide, formic acid, or methanol was used with 125 cm^3/min of steam, 100 cm^3/min of hydrogen, and 10 cm^3/min of nitrogen.

2.6.1.2. Kinetic isotope effect measurements in the fixed-bed reactor Hydrogen was not included in the feed for experiments for assessing the presence of a kinetic isotope effect. Only steam (125 cm^3/min) and the reactant of interest (carbon monoxide, formic acid, or methanol, 3.75 cm^3/min) were included. During WGS, $D_2O + CO$ was switched to $H_2O + CO$; during water-assisted formic acid decomposition, $DCOOH + H_2O$ was switched to $HCOOH + H_2O$; and during methanol steam reforming, $CD_3OD + D_2O$ was switched to $CH_3OH + H_2O$. In each case, the temperature was adjusted to ensure that the measurements were carried out in the kinetically limited regime.

2.6.1.3. In situ DRIFTS For each set of experiments, the catalyst was first treated in pure O_2 (100 cm^3/min) at 400 °C for 12 h. For WGS, surface coverage was monitored under steady-state reaction conditions. In these tests, the catalyst was first treated with either 100 cm^3/min of H_2 or D_2 at 300 °C, followed by a N_2 purge. The WGS reaction was run at 250 °C with $CO + H_2O$ (or D_2O) using 3.75 cm^3/min CO:125 cm^3/min H_2O:10 cm^3/min N_2 at steady state, and the formate coverage was determined. After WGS, the sample was steamed and purged with N_2. CO adsorption was then performed to assess the formate coverage at the same partial pressure and space velocity as done during the steady-state reaction condition, with N_2 (135 cm^3/min) serving as the balancing gas. The dynamic response of the formate surface coverage with temperature was assessed by running the same test at 300 °C.

2.6.2. In situ DRIFTS adsorption and transient decomposition measurements

2.6.2.1. Catalyst activation Two routes of bridging OH group activation were tested. First, as before, the catalyst was treated using pure O_2 at 400 °C. Then the catalyst was activated using 100 cm^3/min H_2 at 300 °C (or 100 °C). In a separate test, the O_2-calcined catalyst was activated with

a mixture of 3.75 cm^3/min CO and 135 cm^3/min N_2 at 300 °C, followed by steaming with 125 cm^3/min of H_2O. The formation and decomposition of adsorbed species were followed by in situ DRIFTS, and the bridging OH band intensity was examined for each case. Scans were made after cooling in N_2 to 100 °C.

2.6.2.2. Transient WGS After steady-state WGS, the sample was steamed and purged with N_2 and cooled to 160 °C. CO adsorption was carried out using 3.75 cm^3/min CO and 135 cm^3/min N_2. The stabilized formate was then decomposed by reaction with H_2O (125 cm^3/min), and the formate decomposition/CO_2 evolution followed. The sample was purged with N_2, and then CO was readsorbed.

2.6.2.3. Formic acid adsorption After reduction in H_2 at 300 °C, the sample was purged with N_2 and cooled to 160 °C. Formic acid was adsorbed by bubbling N_2 through a saturator containing the pure liquid.

2.6.2.4. Transient methanol steam reforming After reduction in H_2 at 300 °C, the sample was purged with N_2 and cooled to 160 °C. Methanol was adsorbed by bubbling N_2 through a saturator containing the pure liquid held at room temperature. The sample was purged with N_2, and then H_2O was flowed to evaporate at a temperature slightly higher than that of the infrared cell, and the decomposition of methanol followed.

2.7. High-resolution transmission electron microscopy

High-resolution transmission electron microscopy (HRTEM) measurements were carried out using a JEOL 2010F FasTEM field emission electron microscope, equipped with an energy dispersive X-ray detector and operated at an accelerating voltage of 200 kV. The electron beam had a point-to-point resolution of 0.5 nm. Calcined, unpromoted thoria powder was lightly dusted onto 200-mesh Cu grids coated with lacy carbon.

3. Results

3.1. H_2 treatment of Pt/thoria: TPR, thermogravimetric analysis-mass spectroscopy, and XANES

First, thoria was treated with hydrogen in an in situ flow cell from room temperature to 500 °C. Normalized XANES spectra as a function of temperature for the unpromoted and 1% Pt-promoted thoria catalysts are reported in Figs. 1a and b, and the edge onset changes are provided for each XANES spectrum, referenced to the room temperature spectrum. For unpromoted thoria, the results indicate that little, if any, change occurred in the temperature range explored. However, when 1 wt% Pt was added to thoria, important changes were noted in the low-range WGS temperature (between 200 and 300 °C). A slight decrease in white line intensity was seen at 200 °C, but further increases in temperature did not affect the intensity; rather, a significant decrease in the edge position to lower eV was observed. By 300 °C, the decrease in the onset of the edge jump shifted downward approximately 0.8 eV, whereas by 400 °C, the shift was more pronounced—about 1.3 eV relative to the unreduced spectrum. Increasing the temperature to 500 °C did not shift the spectrum further. The results show good agreement with our previously reported TPR measurements for thoria [1]. Uptake of hydrogen was observed in the 200–400 °C range for the Pt-promoted thoria catalyst, with less hydrogen uptake for unpromoted thoria at >400 °C.

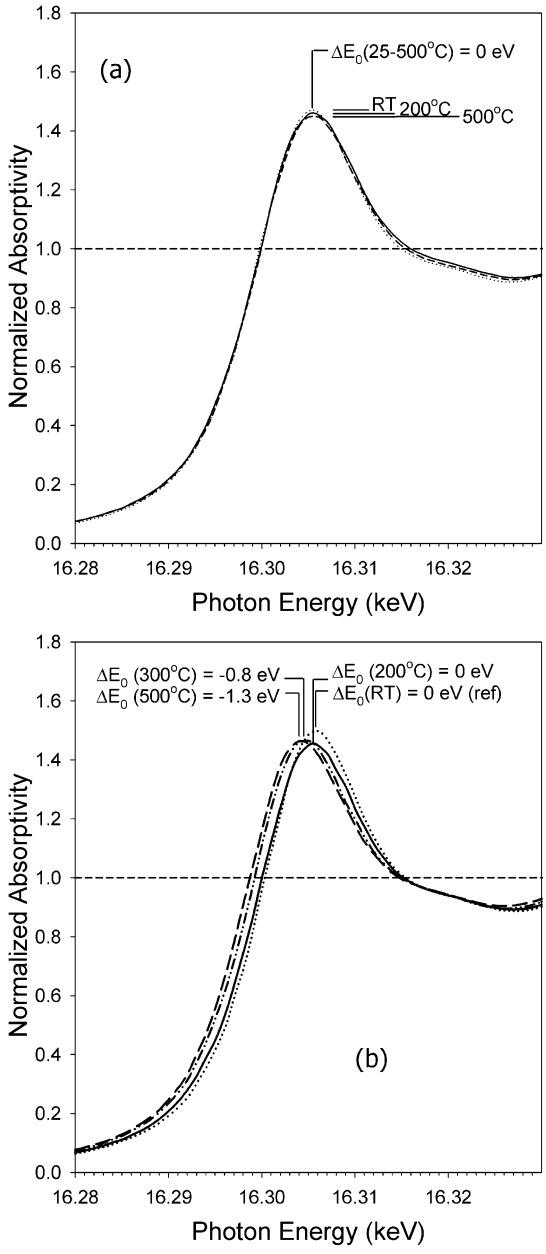

Fig. 1. Normalized XANES profiles of (a) unpromoted and (b) Pt-promoted thoria catalysts as a function of temperature, under H_2 treatment using H_2:He (150 cm^3/min:500 cm^3/min).

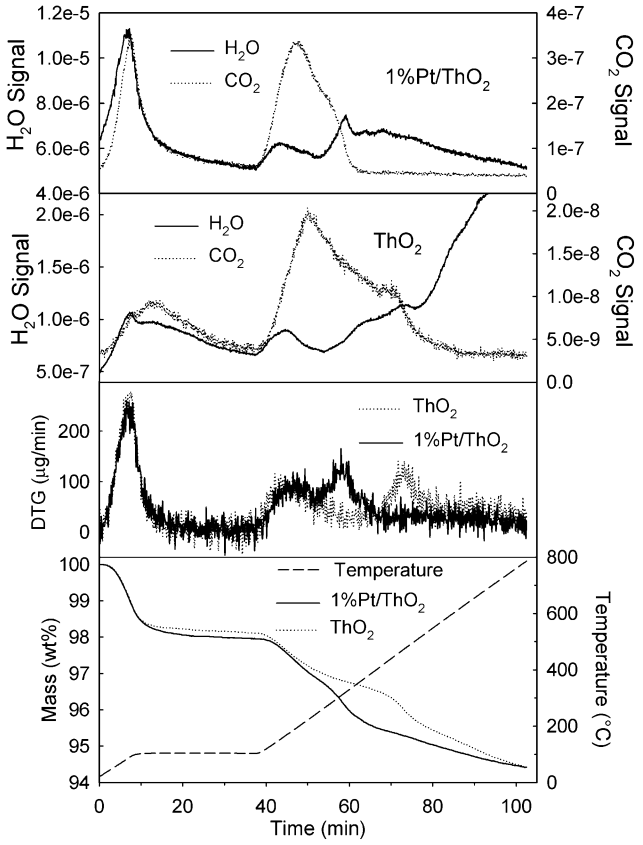

Fig. 2. (Bottom) mass loss profiles, (middle) differential thermal gravimetric scans, and (top two) mass spectrometer results, for unpromoted thoria and Pt/thoria catalysts.

Thermogravimetric analysis–mass spectroscopy (TGA-MS) results are displayed in Fig. 2. Thermal treatment in flowing hydrogen reveals a more rapid decrease in mass for the Pt/thoria catalyst than for unpromoted thoria, evolving H_2O ($m/e = 18$) and CO_2 ($m/e = 44$) during the reduction process. For Pt/thoria, CO_2 evolved until a temperature between 300 and 350 °C was obtained, whereas much higher temperatures (ca. 550–600 °C) were needed to accomplish this for the unpromoted catalyst. For both unpromoted and Pt-promoted thoria, H_2O evolution included a peak below 200 °C attributed to desorption of the physisorbed H_2O from the surface. However, at higher temperatures, a broad peak was observed for unpromoted thoria over the range 350–600 °C, whereas a sharp peak at a lower temperature (ca. 300 °C) was obtained for the Pt-promoted catalyst. The data suggest that Pt facilitates the decomposition of surface carbonates as CO_2 through decarboxlation occurring during the catalyst surface shell reduction process.

3.2. Isotopic studies using in situ DRIFTS and reaction tests

3.2.1. Formation of the type II bridging OH groups

3.2.1.1. Hydrogen activation The catalyst was first treated in O_2 at 400 °C, as discussed previously. The DRIFTS spectra (Fig. 3) show the changes to the catalyst during activation in hydrogen at 300 °C. As shown, bands in the region 1200–1600 cm^{-1}, consistent with the asymmetric and symmetric stretching OCO vibrations of carbonate, disappear while a band at 2140 cm^{-1} develops and then disappears. The latter band is likely associated with desorption of CO from the catalyst surface. The single-beam intensity data reported in Fig. 4 give a good indication of the extent of carbonate removal from the catalyst; the figure compares the Pt/thoria after the hydrogen treatment with that of the freshly loaded catalyst and the O_2-calcined catalyst.

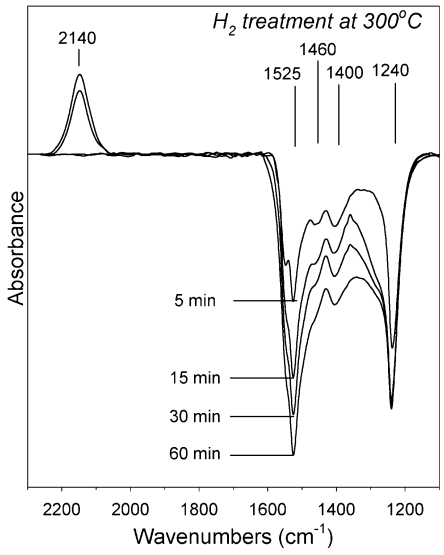

Fig. 3. DRIFTS spectra as a function of time during H_2 treatment (100 cm^3/min) at 300 °C. Spectra referenced to the spectra taken after O_2 treatment (100 cm^3/min) at 400 °C, and cooled to 300 °C in N_2.

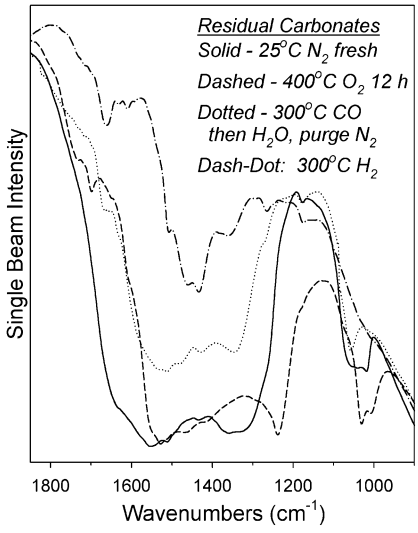

Fig. 4. DRIFTS single beam intensity spectra displaying residual carbonate for (—) the fresh catalyst at room temperature; (- - -) after O_2 calcination (100 cm^3/min) at 400 °C for 12 h; (-·-·-) after H_2 treatment (100 cm^3/min) at 300 °C; and (···) after CO:N_2 treatment (3.75 cm^3/min:135 cm^3/min) at 300 °C, followed by H_2O:N_2 treatment (125 cm^3/min:10 cm^3/min), and then a final N_2 purge (135 cm^3/min).

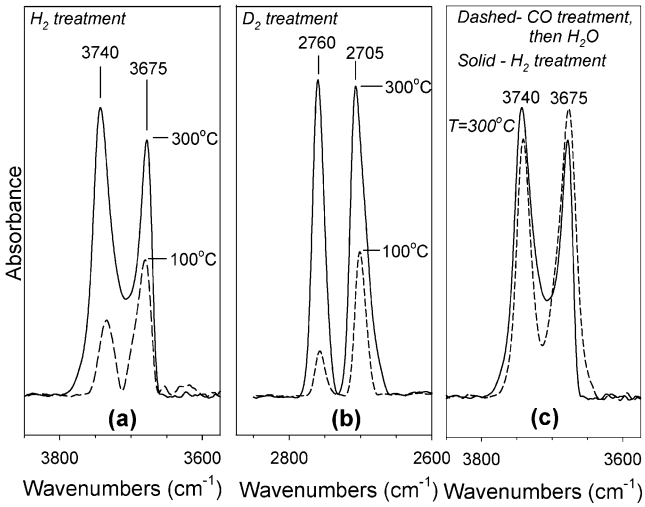

Fig. 5. DRIFTS spectra of bridging OH group bands (a) after H_2 treatment (100 cm^3/min), (b) after D_2 treatment (100 cm^3/min), and (c) a comparison of the catalyst after (solid) H_2 treatment (100 cm^3/min) at 300 °C or (- - -) after CO:N_2 treatment (3.75 cm^3/min:135 cm^3/min) at 300 °C, followed by H_2O treatment (125 cm^3/min:10 cm^3/min), and then a final N_2 purge (135 cm^3/min). All of the scans were taken after cooling to 100 °C in N_2 and are referenced to the fresh catalyst after O_2 treatment (100 cm^3/min) at 400 °C, and cooled to 100 °C in N_2.

Fig. 5 indicates the development of bands at 3675 and 3740 cm^{-1} associated with OH or OD groups on the surface of thoria after treatment at either 100 or 300 °C (cooled to 100 °C in N_2). Higher-temperature treatment in hydrogen (or deuterium) increases the density of the OH (OD) groups on the surface.

3.2.1.2. Carbon monoxide, followed by steaming activation

A fresh calcination was conducted (400 °C in O_2). Figs. 6a and 6b show the bands that disappear and evolve during activation in CO at 300 °C. It is evident that bands near 1530 and 1240 cm^{-1} associated with carbonate ν(OCO) asymmetric and symmetric vibrations essentially disappear, whereas those at 1585 and 1370 cm^{-1} associated with asymmetric and symmetric ν(OCO) vibrations of formates evolve. The latter are accompanied by the formation of bands in the C–H stretching region associated with surface formates (main band at 2860 cm^{-1}, with minor bands at 2950 and 2725 cm^{-1}). Although there is no question that the band at 2860 is assigned to ν(C–H), the precise assignment of the minor bands remains unclear. Binet et al. [9] assigned analogous bands on ceria to the combination δ(C–H) + ν_s(OCO) and the overtone 2δ(C–H), respectively. Others have assigned the minor bands to differently coordinated (e.g., bridged) formates. There are also bands that form and decrease at 2180 and 2125 cm^{-1}, respectively. Again, as with ceria, these are likely assigned to ν(CO) stretching for CO adsorbed on thoria. In the case of unreduced ceria, on CO adsorption, a band positioned at 2168 cm^{-1} was reported that was very similar to the high-wavenumber band observed with thoria and was ascribed to ν(CO) stretching for CO adsorbed on Ce^{4+} cations [22,23]. This explanation appears

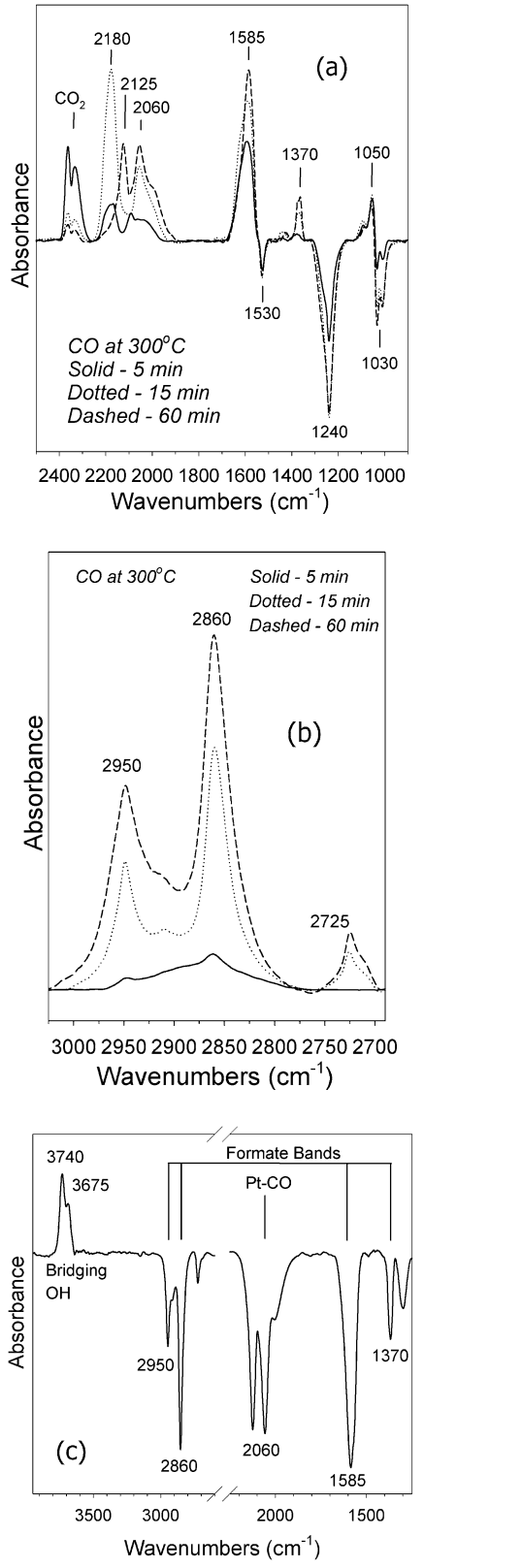

Fig. 6. DRIFTS spectra taken during CO:N_2 treatment (3.75 cm^3/min:135 cm^3/min) at 300 °C (a) in the region between 1000 and 2500 cm^{-1}; (b) in the region between 2700 and 3100 cm^{-1}; and (c) after switching to H_2O:N_2 (125 cm^3/min:10 cm^3/min) at 300 °C. Spectra referenced to the spectra taken after O_2 treatment (100 cm^3/min) at 400 °C, and cooled to 300 °C in N_2.

suitable for the Pt/thoria catalyst as well. Interestingly, for partially reduced ceria, a band was reported at 2126 cm^{-1} possibly due to ν(CO) stretching for CO adsorbed on Ce^{3+} cations [22] occurring at reduced centers (i.e., oxygen vacancies). The development of the 2125 cm^{-1} band observed for thoria likewise suggests ν(CO) stretching for CO adsorbed on thoria at oxygen-deficient sites. Bands between 1900 and 2060 cm^{-1} are also associated with ν(CO) stretching, but in this case for CO adsorbed on the Pt surface.

As shown in Fig. 6c, after partial reduction with CO, addition of H_2O led to the removal of bands assigned to formate, Th–CO, and Pt–CO. Subsequently, strong bands developed at 3675 and 3740 cm^{-1}, attributed to the OH groups on thoria observed previously with H_2 treatment. Fig. 4 shows that the intensity of residual carbonate species after activation by the CO, followed by H_2O, procedure, was somewhat higher in concentration than was observed by the H_2 activation procedure.

Interestingly, however, as demonstrated in Fig. 5c, both activation procedures yield the same OH bands with almost identical intensities. Spectra were measured after cooling to 100 °C in nitrogen flow. Therefore, the results indicate that in a fuel processor for low-temperature WGS, where flows of hydrogen and water are considerably higher than the flow of carbon monoxide, bridging OH groups are an important potential active site. The bridging OH groups are associated with reduced centers on the surface of thoria, just as in the case of Pt/ceria.

3.2.2. *WGS and relationship to water-assisted formic acid decomposition*

Fig. 7 shows that the type II bridging OH groups react with CO to generate surface formate bands that are virtually identical to those reported in our work with Pt/ceria [13–15] and reported by Shido and Iwasawa [12]. The formates are quite stable at 160 °C but decompose readily when H_2O is introduced. We have recently commented on the importance of the reactant-promoted (i.e., water-promoted) formate decomposition in isotope-switching studies using ^{13}C-labeled CO for forward shift and ^{13}C-labeled CO_2 for the RWGS. The importance of including H_2O in the formate decomposition was noted by Shido and Iwasawa [12], who included water in the transient state of the formate decomposition elementary step. The Pt–CO band also decreased, although not as extensively as that of the formate. The catalyst was purged after the water-assisted formate decomposition step with nitrogen, then CO was reintroduced. Again, the formates were produced. Fig. 8 indicates that during steady-state WGS, the formate bands become limited on the surface, suggesting that they are controlled by the WGS reaction rate. In contrast, the band intensity of Pt–CO did not change considerably. Both findings are in agreement with our past studies with Pt/ceria [13]. We have concluded that a formate mechanism is likely operating for WGS, due to kinetic considerations, for both materials. That is, kinetic studies with metal/ceria catalysts have revealed that with high H_2O/CO

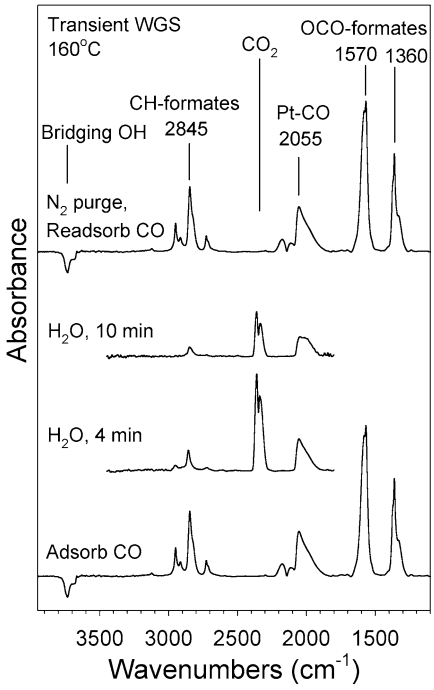

Fig. 7. DRIFTS spectra taken after CO adsorption with CO:N_2 (3.75 cm^3/min:135 cm^3/min) at 160 °C and after switching to H_2O:N_2 (125 cm^3/min:10 cm^3/min) at 160 °C. Readsorption of CO was conducted after purging the steam with N_2 (135 cm^3/min).

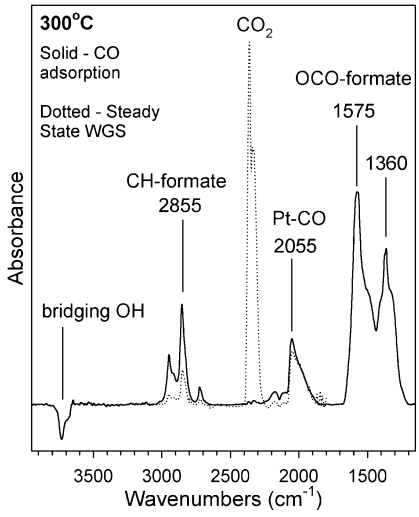

Fig. 8. DRIFTS spectra taken at 300 °C (···) during steady state WGS testing using a mixture of CO, H_2O, and N_2 (3.75 cm^3/min, 125 cm^3/min, and 10 cm^3/min) and (solid) after purging with N_2 (135 cm^3/min), and then conducted CO adsorption using CO:N_2 (3.75 cm^3/min:135 cm^3/min). Spectra referenced to the H_2 treated sample at 300 °C.

ratios, typical of a fuel processor for low-temperature WGS, the rate of the reaction exhibits a first-order dependency with respect to CO and a zero-order dependency with respect to H_2O [18], and vice versa for high CO/H_2O ratios. These results imply the existence of an adsorbed H_2O species at high H_2O/CO ratios that is close to saturation during WGS, and that the concentration of the adsorbed CO intermediate is

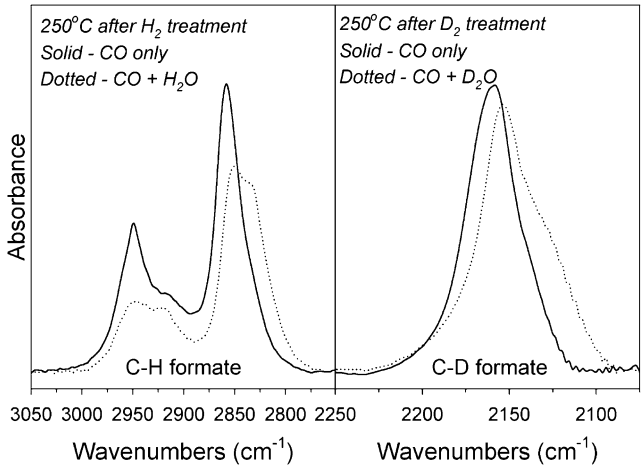

Fig. 9. DRIFTS spectra revealing the normal kinetic isotope effect associated with surface formate coverage. Dotted line displays the C–H (or C–D) formate bands during steady state WGS at 250 °C with a mixture of CO, steam (i.e., H_2O or D_2O), and N_2 (3.75 cm^3/min:125 cm^3/min:10 cm^3/min). Solid line displays the formate band after switching off steam, purging with N_2 (135 cm^3/min), and conducting CO adsorption with CO:N_2 (3.75 cm^3/min:135 cm^3/min).

controlled by the WGS rate. We thus can conclude that in both cases, the adsorbed H_2O species are the type II bridging OH groups, and the appropriate adsorbed CO intermediate is a formate species.

There is additional evidence indicating that this is the case. Fig. 9 shows that the formate bands corresponding to ν(CH) become more reaction rate-limited during WGS than those associated with ν(CD) when D_2O is used. In both cases, the total number of adsorption sites available is simply measured by stopping WGS, purging the water out with N_2, and then adsorbing CO. The ratio of the coverages $\theta_{D_2O}/\theta_{H_2O}$ during WGS with either H_2O or D_2O reveals a normal kinetic isotope effect (NKIE) of 1.3. This is the same NKIE observed in the CO conversion when switching from H_2O to D_2O in fixed-bed reactor testing, as shown in Fig. 10a. Results are analogous to those reported for studies with Pt/ceria [24].

Fig. 11 shows that formic acid dissociates on the surface of partially reduced thoria to generate bands for the same formate species as is produced from the adsorption of CO to the type II bridging OH groups. Relevant to the previous dis-

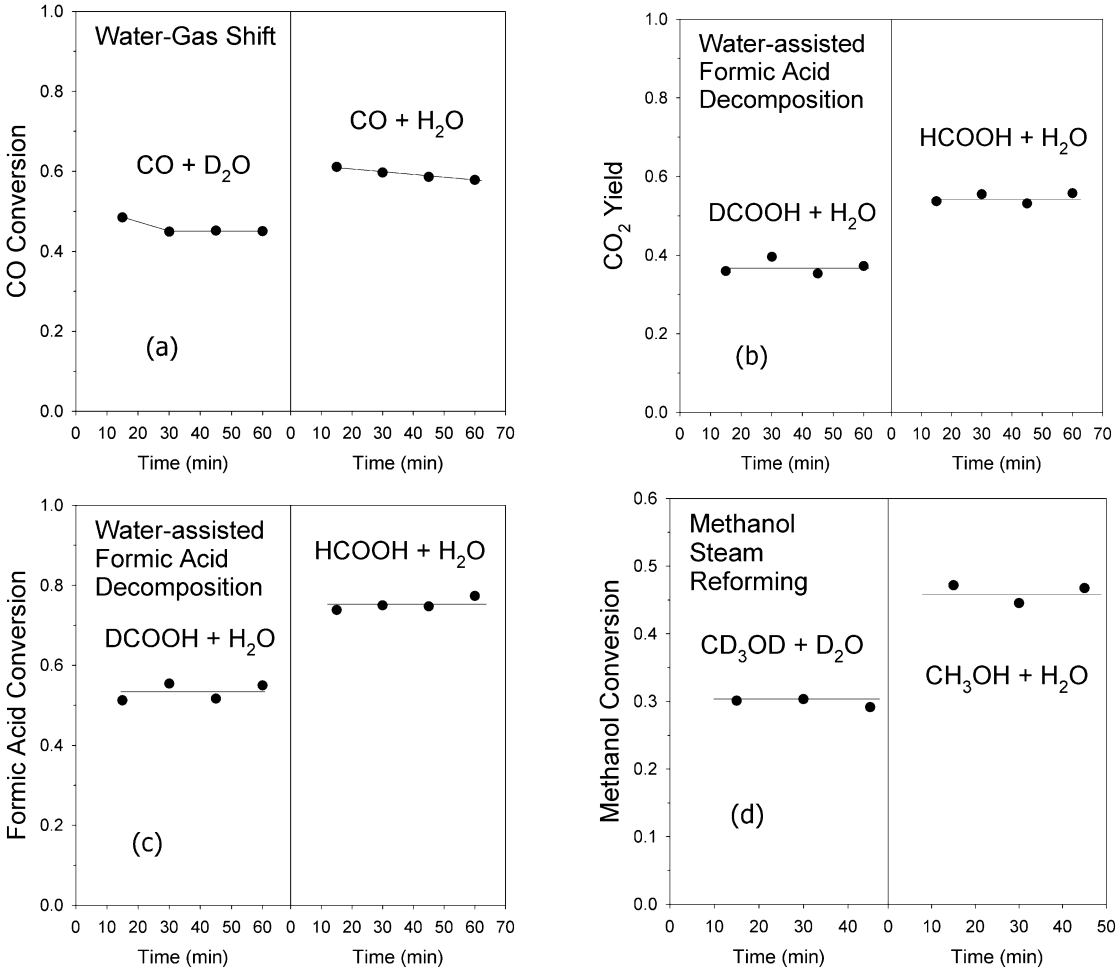

Fig. 10. Results of reaction tests in a fixed bed reactor. Normal kinetic isotope effect for (a) water–gas shift from H_2O:D_2O switching; (b and c) water-assisted formic acid decomposition switching between HCOOH + H_2O and DCOOH + H_2O; and (d) methanol steam reforming switching between CD_3OD + D_2O and CH_3OH + H_2O.

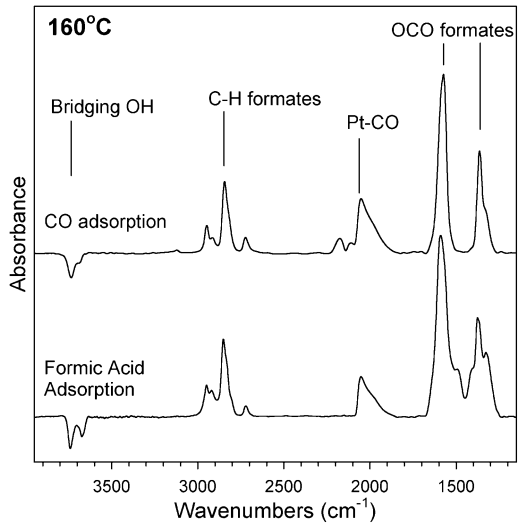

Fig. 11. DRIFTS spectra comparison of bands evolved after CO adsorption using CO:N_2 (3.75 cm^3/min:135 cm^3/min), and after formic acid adsorption using N_2 bubbled through a saturator containing HCOOH. Spectra referenced to the catalyst after O_2 calcination (100 cm^3/min) at 400 °C and H_2 treatment (100 cm^3/min) at 300 °C, cooled to 160 °C in N_2 (135 cm^3/min).

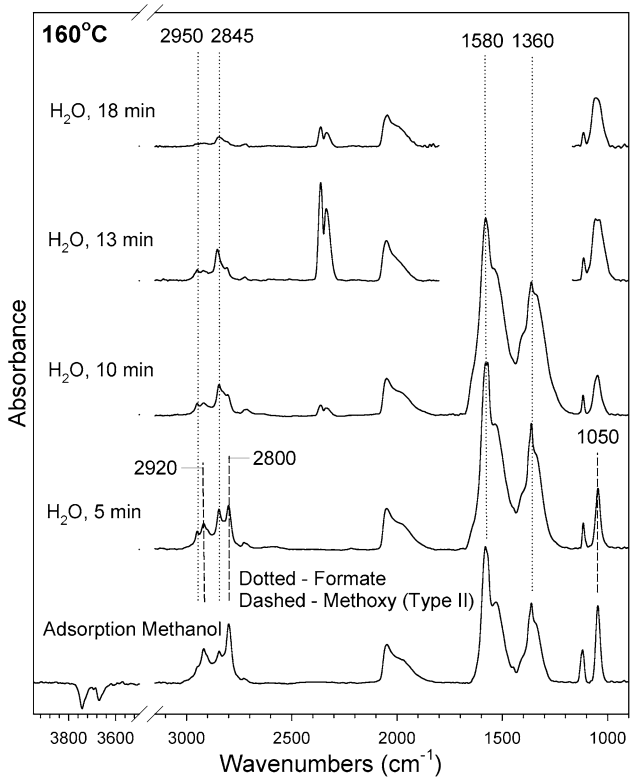

Fig. 12. DRIFTS spectra for the adsorption of methanol using N_2 bubbled through a saturator containing CH_3OH, and after switching to H_2O using H_2O:N_2 (125 cm^3/min:10 cm^3/min) and following the evolution of adsorbed species with time. Spectra referenced to the catalyst after O_2 calcination (100 cm^3/min) at 400 °C and H_2 treatment (100 cm^3/min) at 300 °C, cooled to 160 °C in N_2 (135 cm^3/min).

cussion on the WGS mechanism is the hypothesis that C–H bond scission of formate is the rate-limiting step of the reaction mechanism, as proposed by Shido and Iwasawa [12]. We examined the impact on formic acid conversion in a highly H_2O-concentrated feed by switching from H-labeled to D-labeled formic acid (i.e., switching from HCOOH to DCOOH). As shown in Figs. 10b and 10c, here again is a NKIE of about 1.35 for the conversion of formic acid. These results indicate a strong link between the mechanisms of water-assisted formic acid decomposition and that of WGS and demonstrate the importance of both type II OH groups and formates in these mechanisms.

3.2.3. Steam reforming of methanol

Steam reforming of methanol was also examined by DRIFTS. Methanol was adsorbed on the partially reduced form of Pt/thoria, accompanied by a decrease in the type II bridging OH group bands and the evolution of major bands for methoxy species, ν(OC) at 1050 cm^{-1} and ν(CH) at 2700–3000 cm^{-1}, including identifying bands at 2800 and 2920 cm^{-1}. Surface formates were also present, including ν(OCO) at 1580 and 1360 $cm^{-1}$and ν(CH) at 2845 and 2950 cm^{-1}, although these bands were much weaker in intensity than those observed for CO adsorption and formic acid dissociation.

Returning to the methoxy species, Binet et al. [9] identified two distinguishing types on ceria depending on whether or not the surface was reduced. Type I species, occurring on unreduced ceria, are distinguished by a band in the range 1106–1112 cm^{-1}, whereas an entirely different band position was reported when methanol was adsorbed after surface shell reduction. In keeping with the nomenclature, the band for the latter species was reported at ca. 1060 cm^{-1} and assigned to a type II methoxy species. It is evident that with the Pt/thoria catalyst, adsorption after the H_2 reduction treatment generated two bands, one at 1050 cm^{-1} and another at ca. 1110 cm^{-1}, and we tentatively assign these to adsorption on the surface of thoria, with different degrees of coordinative unsaturation of cationic sites. That is, we suggest that the surface is partially reduced, in agreement with the XANES data. The relative ratio of the type II to type I bands indicates that the unsaturated cationic sites predominate after the reduction procedure, which is catalyzed by the presence of Pt.

With water addition, bands responsible for the methoxy species (i.e., 1050, 1110, 2800, and 2920 cm^{-1}) decreased, whereas those of the surface formates (1580, 1360, 2845, and 2950 cm^{-1}) increased significantly, suggesting a conversion process (Fig. 12). Only when the formates reached a maximum was gas phase CO_2 observed. The band for gas phase CO_2 reached a maximum during formate decomposition and diminished considerably when the formate band had nearly disappeared. As in the case of transient WGS, a considerable band for Pt–CO remained, suggesting that formates likely act as intermediates in the methanol steam reforming reaction. Interestingly, as shown in Fig. 13, the residual carbonate bands, after purging out the H_2O with N_2, were virtually identical to those after the transient WGS experiment. The DRIFTS experiment again highlights the

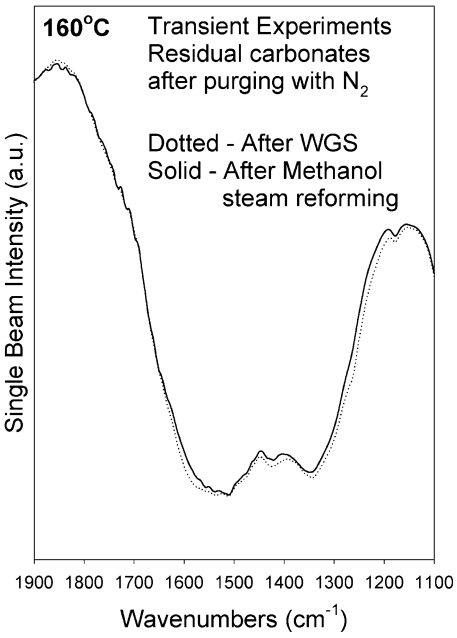

Fig. 13. Residual carbonate species after purging H_2O with N_2 (135 cm^3/min) following the transient DRIFTS experiments at 160 °C of (···) formate decomposition from water–gas shift (Fig. 8) and (—) methoxy and formate species decomposition from methanol steam reforming (Fig. 11).

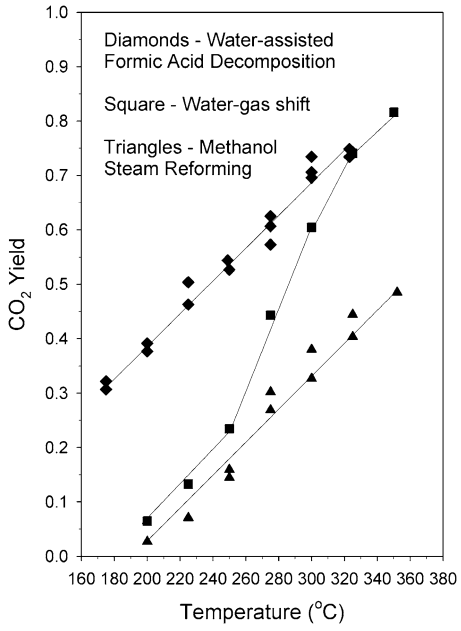

Fig. 14. CO_2 yield versus temperature curves over Pt/thoria for (◆) formic acid decomposition; (■) low-temperature water–gas shift; and (▲) methanol steam reforming. Conditions: 3.75 cm^3/min of either CO, HCOOH, or CH_3OH, 125 cm^3/min H_2O, 100 cm^3/min H_2, and 10 cm^3/min N_2, 33 mg catalyst.

importance of the adsorbed bridging (i.e., type II) species, as well as the role of formates, in catalysis. A potential kinetic isotope effect was probed in switching between $CD_3OD + D_2O$ and $CH_3OH + H_2O$; the result was approximately 1.55 (Fig. 10d), higher than that detected by either WGS or water-assisted formic acid decomposition but measurably lower than the value of 1.75 that we reported [25] for methanol steam reforming over Pt/ceria.

Activity data for the three reactions over Pt/thoria are reported in Fig. 14. In agreement with the literature, the rates, as measured by CO_2 yield, follow in this order: water-assisted formic acid decomposition > WGS > methanol steam reforming. Of greater interest from the standpoint of H_2 production is a comparison on the basis of selectivity between Pt/thoria and Pt/ceria, reported in Figs. 15a–15c. Not only was Pt/thoria more active than Pt/ceria on the basis of methanol conversion, but also the catalyst was more selective for CO_2 relative to CO at higher conversion. CO_2 selectivity is plotted versus both temperature and conversion.

3.3. *Nanoarchitecture of thoria*

HRTEM images of the thoria nanostructure are presented in Fig. 16. The thoria domains display a high degree of nanocrystallinity and have an average size of approximately 3–5 nm. The growth of the crystallite array appears to follow a rod-like mechanism, with subsequent three-dimensional growth resulting in a weblike macrostructure and a corrugated surface with repeating ridges.

4. Discussion

The XANES, DRIFTS, and kinetic isotope effect experiments provide insight into the nature of the active sites operating for Pt/thoria, and mechanisms can be postulated for the three reactions of interest. On the basis of the XANES findings, Pt promotes partial reduction of thoria in a manner analogous to that of ceria, thereby generating type II bridging OH groups on the surface that are associated with coordinatively unsaturated Th cations. The TGA-MS results and DRIFTS measurements support the conclusion that OH group formation occurs in conjunction with the removal of surface carbonates, and thus Pt plays an important role in facilitating decarboxylation during activation.

It is important to consider that for ceria, when oxygen deficiencies are formed, or the bridging OH groups associated with the dissociation of H_2O at those vacancies, two phenomena are observed by XANES at the L_{III} edge. As discussed in previous work [15], when ceria is treated with H_2, the white line shape changes remarkably during reduction. For Ce^{4+}, there are two major peaks, C and B_1. In terms of the final state configuration, peak C corresponds to $Ce[2p^5 4f^0 5d^1]O[2p^6]$, whereas peak B_1 is usually written as $Ce[2p^5 4f^1 5d^1]O[2p^5]$. Peak B_0, in contrast, is indicative of Ce^{3+}, and its final state configuration is normally written as $Ce[2p^5 4f^1 5d^1]O[2p^5]$. It is clear from our previous work [15] that for the Pt/ceria catalyst, only a partial reduction occurs, because the spectrum is clearly a combination of the two states (i.e., two different white line shapes). Peak

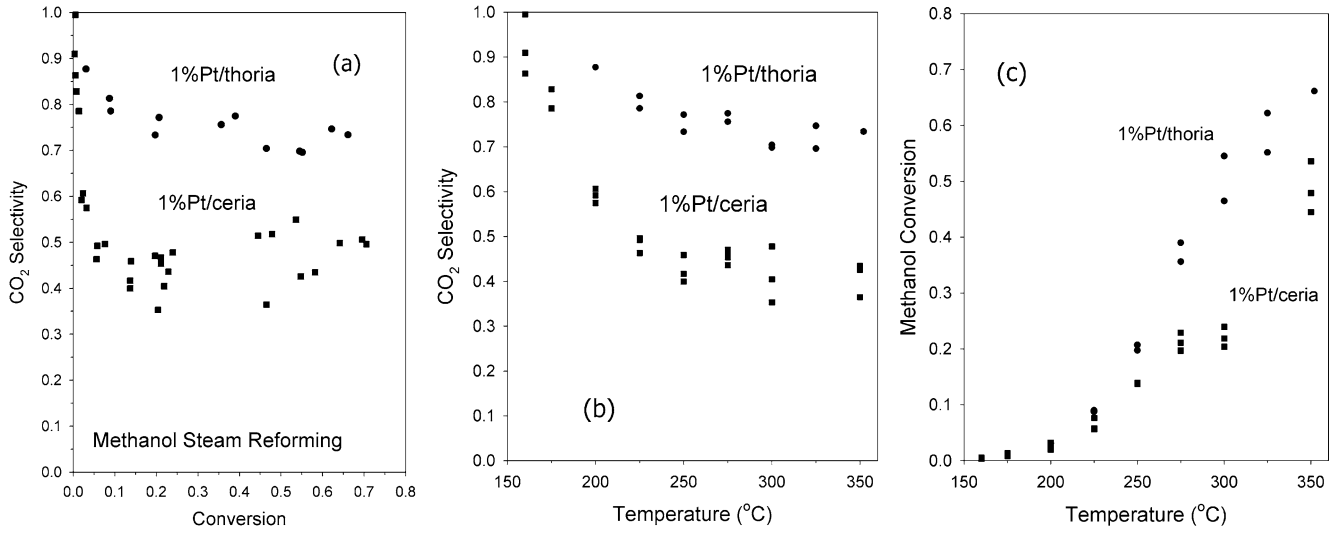

Fig. 15. Steam reforming of methanol—(a) CO_2 selectivity versus conversion; (b) CO_2 selectivity versus temperature; and (c) methanol conversion versus temperature curves for (●) Pt/thoria and (■) Pt/ceria catalysts. Conditions: 3.75 cm^3/min of CH_3OH, 125 cm^3/min H_2O, 100 cm^3/min H_2, and 10 cm^3/min N_2, 33 mg catalyst.

C was observed to decrease, whereas peak B shifted to lower energy at the B_0 position. Because B_0 was situated at lower energy, reduction caused the general lowering of the edge position (related to the binding energy) commonly observed during reduction. The bridging OH groups associated with the surface Ce^{3+} atoms were clearly observed to form using infrared spectroscopy.

In contrast, Th^{4+} is quite difficult to reduce, and Th^{3+} has not been reported in the temperature range of interest. Interestingly, however, ThI_3 has been synthesized, but it is generally interpreted to be [Th^{4+}, $3I^-$, e^-] [26]. To maintain charge balance associated with reduced centers (i.e., vacancies) in the surface of thoria, a formal charge of Th^{3+} can be assigned. However, vacancies can be generated without a real change in oxidation state of thoria from 4+ to 3+. When doing this, one must consider the aforementioned delocalized electron model, which may result in increased electron density associated with the surface O atoms involved in the bridging OH groups. Certainly, the OH groups are considered highly basic. Considering the foregoing factors, we would not expect to observe large changes in the white line shape for thoria during reduction, because it is not truly Th^{3+}. Rather, we would expect a decrease in the binding energy due to the presence of the delocalized electron, as a result of enhanced core-hole shielding. A shift in binding energy E_0 to lower energy is suggested by a decrease in the edge energy position observed at the Th L_{III} edge. Clearly, thoria may become nonstoichiometric for O at the surface during reduction. Yet it is also important to note that, based on the activation experiments, in the presence of H_2 or after CO reduction and steaming, bridging OH groups are formed that are associated with the reduced centers, in a manner similar to ceria, as follows for one possible scheme:

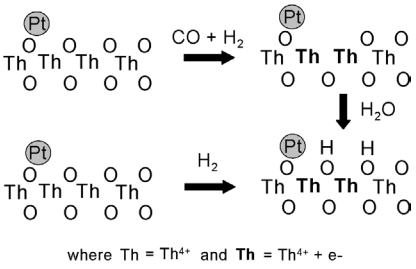

(3)

Both CO adsorption and formic acid dissociation generate surface formates, with the latter process involving liberation of H_2O, as follows:

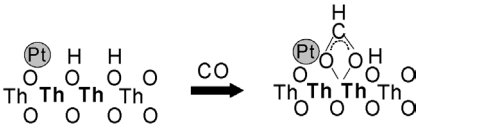

(4)

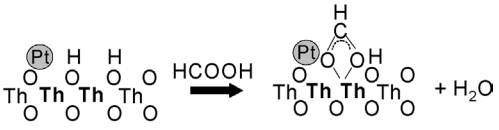

(5)

Based on the DRIFTS results and the NKIE associated with the C–H bond breaking of formate (i.e., rate-limiting step), the following WGS mechanism is proposed, analogous to what has been reported for Pt/ceria [1]:

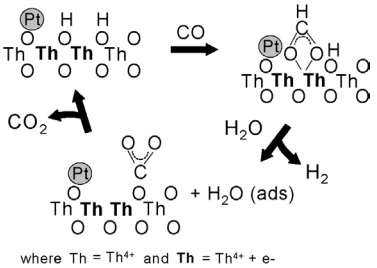

(6)

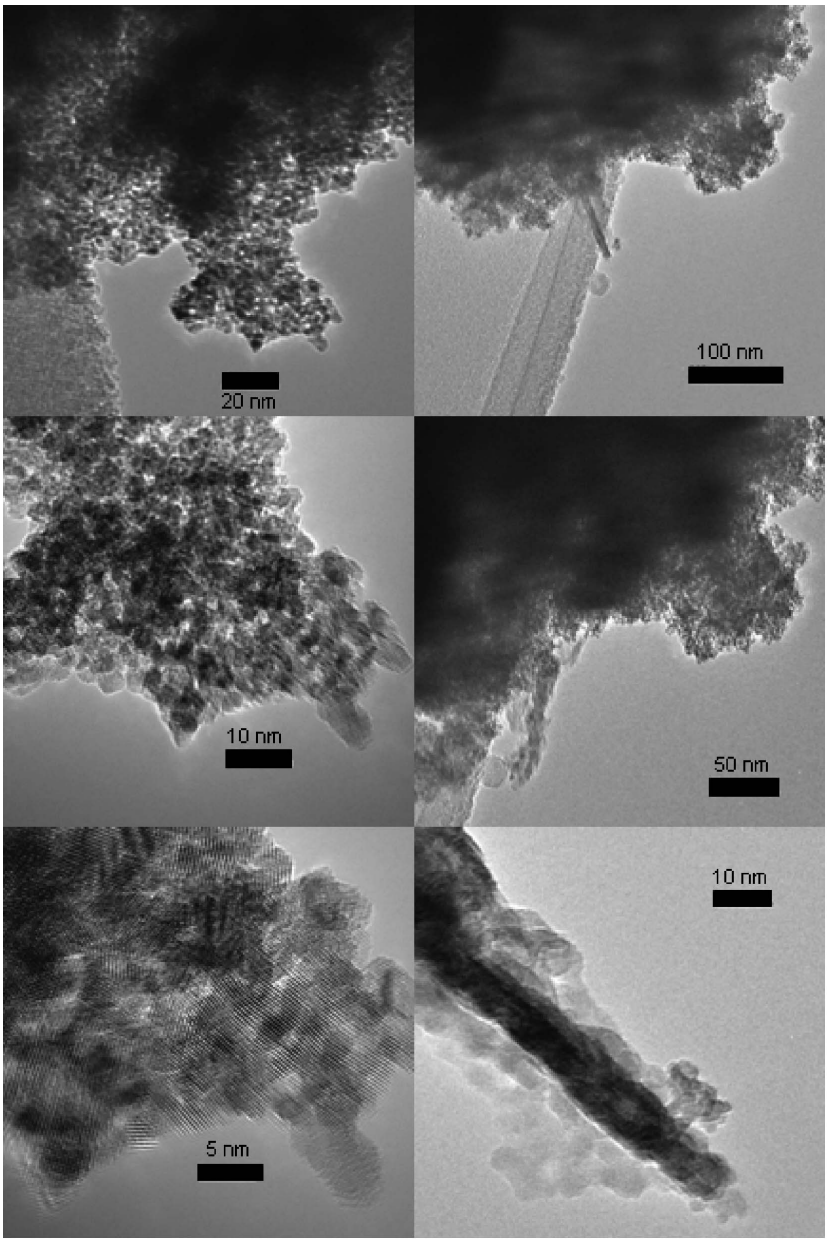

Fig. 16. HR-TEM images of nano-crystalline thoria.

Similarly, formates are proposed to be involved in the methanol steam reforming mechanism, postulated as follows, based on the DRIFTS results:

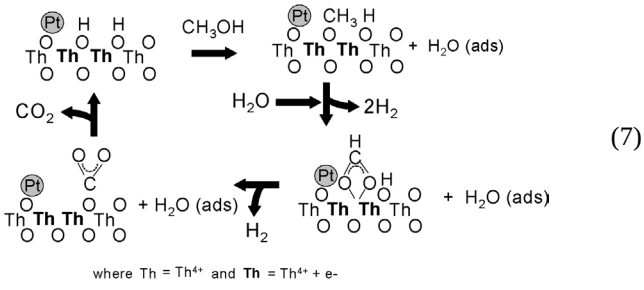

(7)

Methanol steam reforming is currently receiving interest as a means of converting methanol, an important chemical carrier of H_2 that can be produced from a wide variety of fossil fuel and renewable resources. An examination of the CO_2 selectivity versus conversion curves (Fig. 15a) indicates that CO_2 is a primary product and CO is a secondary product. This is an important finding, in that H_2 selectivity thus will be favored at low conversions. Interestingly, the selectivity of CO_2 is higher than that of Pt/ceria even at higher temperatures (and, thus, conversion). These results suggest that methanol steam reforming is in competition with the reverse WGS reaction, as has been postulated for metal/ceria and catalysts containing metal and zirconia promoters [27–29]; that is, CO is generated from the CO_2 produced by catalytic steam reforming. Therefore, one may consider the relative rates of methanol steam reforming and

WGS in terms of the kinetic isotope effect. Although the NKIE associated with formate C–H (C–D) bond cleavage is close to 1.3 for Pt/thoria and close to 1.4 for Pt/ceria, making them essentially equivalent, there is a greater difference in the NKIE associated with steam reforming, which we tentatively conclude is associated with methoxy species decomposition (i.e., also involving C–H bond scission). The NKIE is approximately 1.75 for Pt/ceria and 1.55 for Pt/thoria; therefore, it is not surprising that CO_2 selectivity would be higher during steam reforming for Pt/thoria than for Pt/ceria. It appears that the activation energy barriers associated with methoxy group decomposition and formate decomposition are relatively closer for Pt/thoria than for Pt/ceria. That is, relatively speaking, for Pt/ceria, the methoxy group decomposition is relatively slower, such that CO_2 generated is more rapidly converted to CO through RWGS.

Of course, thoria is a mildly radioactive element, and there are regulatory restrictions associated with its use. However, from the standpoint of abundance, thorium is not at all rare; it comprises 8.1 ppm of the earth's crust. Thus, from the standpoint of hydrogen production at a stationary facility, Pt/thoria is a promising catalyst for use in the production and purification of hydrogen.

5. Conclusions

Previous results suggested that type II bridging OH groups were formed at low temperature for a Pt-promoted thoria catalyst. Because these OH groups are associated with reduced defect centers on the surface of the oxide, direct confirmation of this surface shell reduction process was needed. By comparing XANES spectra for 1% Pt/thoria and unpromoted thoria samples treated in situ in H_2 as a function of temperature, we found that although little reduction occurred for the unpromoted sample in the temperature range explored, remarkable changes occurred for the Pt/thoria catalyst between 200 and 400 °C, including a slight decrease in white line intensity and a pronounced decrease in the onset of the edge jump to lower energy. These findings are consistent with partial reduction due to a fraction of Th atoms with lower oxygen coordination in the surface shell. Partial reduction with H_2 or CO treatment followed by steaming led to the generation of type II bridging OH groups on the surface associated with the reduced centers. DRIFTS experiments and kinetic isotope effect studies point to these OH groups as active sites involved in low-temperature WGS, water-assisted formic acid decomposition, and methanol steam reforming. It has been postulated that at high H_2O/CO ratios, WGS and water-promoted formic acid decomposition pass through surface formate intermediates, whereas methanol steam reforming involves type II methoxy species and formates as intermediates in the pathway. Methanol steam reforming is in competition with RWGS, and CO_2 selectivity is favored at low temperature. Pt/thoria was found to be more selective for methanol steam reforming than a similarly promoted Pt/ceria catalyst. The catalysis of the three reactions investigated appears to be directly analogous to that of Pt/ceria.

References

[1] G. Jacobs, A.C. Crawford, L. Williams, P.M. Patterson, B.H. Davis, Appl. Catal. A: Gen. 267 (2004) 27.
[2] J. Lamotte, J.C. Lavalley, E. Druet, E. Freund, J. Chem. Soc., Faraday Trans. 1 79 (1983) 2219.
[3] J. Lamotte, J.C. Lavalley, V. Lorenzelli, E. Freund, J. Chem. Soc., Faraday Trans. 1 81 (1985) 215.
[4] J. Lamotte, V. Moravek, M. Bensitel, J.C. Lavalley, React. Kinet. Catal. Lett. 36 (1988) 113.
[5] A. Laachir, V. Perrichon, Ad. Badri, J. Lamotte, E. Catherine, J.C. Lavalley, J. El Fallah, L. Hilaire, F. Le Normand, E. Quemere, G.N. Sauvion, O. Touret, J. Chem. Soc., Faraday Trans. 87 (1991) 1601.
[6] C. Binet, A. Badri, J.C. Lavalley, J. Phys. Chem. 98 (1994) 6392.
[7] A. Badri, C. Binet, J.C. Lavalley, J. Chem. Soc., Faraday Trans. 93 (1997) 1159.
[8] A. Badri, C. Binet, J.C. Lavalley, J. Chem. Soc., Faraday Trans. 93 (1997) 2121.
[9] C. Binet, M. Daturi, J.C. Lavalley, Catal. Today 50 (1999) 207.
[10] C. Li, K. Domen, K.-I. Maruya, T. Onishi, J. Catal. 125 (1990) 445.
[11] Y. Iwasawa, T. Shido, J. Catal. 136 (1992) 493.
[12] T. Shido, Y. Iwasawa, J. Catal. 141 (1993) 71.
[13] G. Jacobs, L. Williams, U.M. Graham, D.E. Sparks, B.H. Davis, J. Phys. Chem. B 107 (2003) 10398.
[14] G. Jacobs, P.M. Patterson, L. Williams, D.E. Sparks, B.H. Davis, Catal. Lett. 96 (2004) 97.
[15] G. Jacobs, U.M. Graham, E. Chenu, P.M. Patterson, A. Dozier, B.H. Davis, J. Catal. 229 (2005) 499.
[16] T. Bunluesin, R. Gorte, G. Graham, Appl. Catal. B 15 (1998) 107.
[17] S. Hilaire, X. Wang, T. Luo, R.J. Gorte, J. Wagner, Appl. Catal. 215 (2001) 271.
[18] Q. Fu, A. Weber, M. Flytzani-Stephanopoulos, Catal. Lett. 88 (2001) 87.
[19] D. Tibiletti, A. Goguet, F.C. Meunier, J.P. Breen, R. Burch, Chem. Commun. 14 (2004) 1636.
[20] A. Goguet, F.C. Meunier, D. Tibiletti, J.P. Breen, R. Burch, J. Phys. Chem. B 108 (2004) 20240.
[21] D.A. Skoog, D.M. West, F.J. Holler, Analytical Chemistry, sixth ed., Saunders College Publishing, Philadelphia, 1992, pp. 72–84.
[22] F. Bozon-Verduraz, A. Bensalem, J. Chem. Soc., Faraday Trans. 90 (1994) 653.
[23] C. Li, Y. Sakata, T. Arai, K. Domen, K.I. Maruya, T. Onishi, J. Chem. Soc., Faraday Trans. I 85 (1989) 1451.
[24] G. Jacobs, S. Khalid, P.M. Patterson, D.E. Sparks, B.H. Davis, Appl. Catal. A: Gen. 268 (2004) 255.
[25] G. Jacobs, B.H. Davis, Appl. Catal. A: Gen. 285 (2005) 43.
[26] N.N. Greenwood, A. Earnshaw, Chemistry of the Elements, second ed., Butterworth–Heineman, London, 1997.
[27] A. Mastalir, B. Frank, A. Szizybalski, H. Soerijanto, A.S. Seshpande, M. Niederberger, R. Schomaker, R. Schlogl, T. Ressler, J. Catal. 230 (2005) 464.
[28] J.P. Breen, J.R.H. Ross, Catal. Today 51 (1999) 521.
[29] J.P. Breen, F.C. Meunier, J.R.H. Ross, Chem. Commun. 22 (1999) 2247.